International Journal of Progressive Sciences and Technologies (IJPSAT)
ISSN: 2509-0119.
© 2026 Scholar AI LLC.
https://ijpsat.org/
Vol. 60 No. 1 November 2026, pp. 605-625

Modeling And Evaluation Of A Two-Zone Hybrid Solar System For Steam Production With Electrical Backup: The Case Of Mahajanga, Madagascar

RAHARIJAONA Petera[1], DONA Victorien Bruno[2]

[1]Doctoral student, Doctoral School of Life Engineering and Modeling (EDGVM), University of Mahajanga, Madagascar

[2]Professor, Doctoral School of Life Engineering and Modeling (EDGVM), Applied Physics and Renewable Energy Laboratory (LPADER), University of Mahajanga, Madagascar

Corresponding author: RAHARIJAONA Petera, E-mail: rpetera05@gmail.com; bvdno2@gmail.com

(cc) BY

Abstract: This study analyzes the thermal and electrical performance of a two-zone solar chimney power plant intended to produce steam for essential oil extraction in Mahajanga, Madagascar. The main objective is to evaluate the contribution of a 3 kW auxiliary electric heater during the least favorable month in terms of sunshine. The approach combines meteorological data from 2010–2024 with transient thermal modeling of zone A and modeling of electricity generation in zone B. Simulations for January and October also investigate the influence of electrical power on system performance.

The results show that in October, solar conditions allow zone A to produce 31,57 kg of steam naturally. In January, however, the maximum temperature remains limited to 93,48 °C, preventing the production of the required steam without supplementary input. Zone B generates peak electrical powers of 3,35 kW in January and 4,81 kW in October. Integrating a 3 kW electric heating element allows the saturation temperature to be reached in January and 6,51 kg of steam to be produced over approximately 2 h 12 min, with a maximum flow rate of 4,40 kg.h-1.

Comparison with experimental data identifies Ravintsara as a particularly promising application, although the system studied does not yet meet all its steam requirements. Overall, these findings show that hybrid operation combining solar energy and auxiliary electrical heating is an effective solution for improving steam production and strengthening process continuity during periods of low solar irradiation.

Keywords: solar chimney power plant; hybrid system; auxiliary electrical heating; thermoelectric modeling; steam production; essential oils; Mahajanga.

1. INTRODUCTION

Tropical regions with high sunshine levels, such as northwestern Madagascar (Mahajanga), have substantial solar potential that is often underused in local agro-industrial sectors. Essential oil production currently relies mainly on distillation processes powered by wood or fossil fuels, with considerable environmental impacts and operating costs [1]. Coupling a solar chimney power plant with an extraction process is a little-explored way to harness the local solar resource both for process heat and for the electricity required to operate the installation.

The solar chimney power plant concept combines a greenhouse-effect solar collector, a central chimney and a turbine. Air heated under the collector is accelerated by thermal draft and drives a turbine–generator set. The reference prototype remains the

Manzanares plant (Spain, 1982), with a 194,6 m chimney and a 244 m-diameter collector, which validated the concept at pilot scale but without thermal storage [2].

Previous work on solar collectors with water-based thermal storage, initiated by Kreetz (1997) [3] and extended by SEMAI [4], is based on a nodal formalism describing the collector with seven equations when water storage is present and five without it. In these approaches, storage is treated as an overall property: either present across the entire surface or completely absent, with no intermediate configuration.

To address this limitation, the present study proposes a solar chimney power plant with two functionally distinct zones. The first zone (zone A) is intended for water heating and steam production. The second (zone B) generates electricity through thermal draft. The electricity produced powers a heating element with a rated power of 3 kW, intended to supplement solar heating whenever it becomes insufficient.

The objective of this work is to evaluate the thermal and electrical performance of the two zones and then determine the effect of auxiliary electrical heating on steam production in January. The methodology combines transient thermal modeling, simulation of electricity production, parametric analysis and comparison with experimental extraction trials conducted on Niaouli, Kininina and Ravintsara at the University of Mahajanga.

The study thus aims to characterize the possibilities and limitations of hybrid operation for essential oil extraction, without attempting to optimize the system dimensions at this stage.

2. MATERIALS AND METHODS

2.1. Configuration and operating principle of the system studied

This study proposes a new solar chimney power plant configuration intended to improve the consistency of steam production for essential oil extraction. It extends an earlier study in which the transient model showed that in January, a month with unfavorable solar conditions, the water does not reach saturation, unlike October, when theoretical steam production is obtained. To compensate for this thermal deficit, an architecture combining solar heat production and electricity generation is investigated.

The system comprises two functional zones integrated within a single solar collector (Figure 1). Zone A, dedicated to steam production, consists of a water basin 6 m in diameter containing a 1 cm water layer, at a reference pressure of 1 bar absolute. The basin is fitted with low-emissivity (Low-E) glazing and an immersed electric heating element. It is connected to the still by a thermally insulated steam pipe. Its peripheral location is intended to limit disturbances to the main airflow and shading effects.

Zone B corresponds to the dry portion of the collector. Ambient air enters at its periphery, warms under solar radiation and converges toward the central chimney. Thermal draft drives a turbine coupled to an electric generator. The electricity generated is used to power the zone A heating element, supplementing solar input when it becomes insufficient [5], [6].

Zone B, corresponding to the main dry collector, is described by Kreetz's classical five-equation nodal model [3], adopted by Semai [4] and previously compared with measurements from the Manzanares plant [2]. Since the water basin is physically separated from the main flow, this formulation remains applicable to this zone.

Zone A, consisting of the enclosed water basin, is modeled using thermal phenomena previously studied in solar stills: radiative exchange, natural convection in an enclosed cavity and thermal storage in water. Dunkle [7] established the first correlations for these exchanges in a greenhouse-type still; Hollands et al. [8] refined the calculation of natural convection in an enclosed inclined cavity, a configuration close to that of the basin. These results are reproduced in reference works, particularly Duffie and Beckman, and are applied here without modification, regardless of the basin position.

The two zones thus perform distinct functions but remain linked through energy coupling. Their physical separation is intended to reduce thermal and aerodynamic interactions without assuming complete independence. The electrical power actually available is a constraint on sizing the auxiliary heater.

International Journal of Progressive Sciences and Technologies (IJPSAT)
ISSN: 2509-0119.
© 2026 Scholar AI LLC.
https://ijpsat.org/
Vol. 60 No. 1 November 2026, pp. 605-625

The proposed configuration retains the basin characteristics used in the previous study and introduces a larger electricity-generation zone. The simulations focus mainly on January to determine whether the auxiliary heater can reach saturation and maintain steam production for four hours. October is also considered as a favorable-period operating reference.

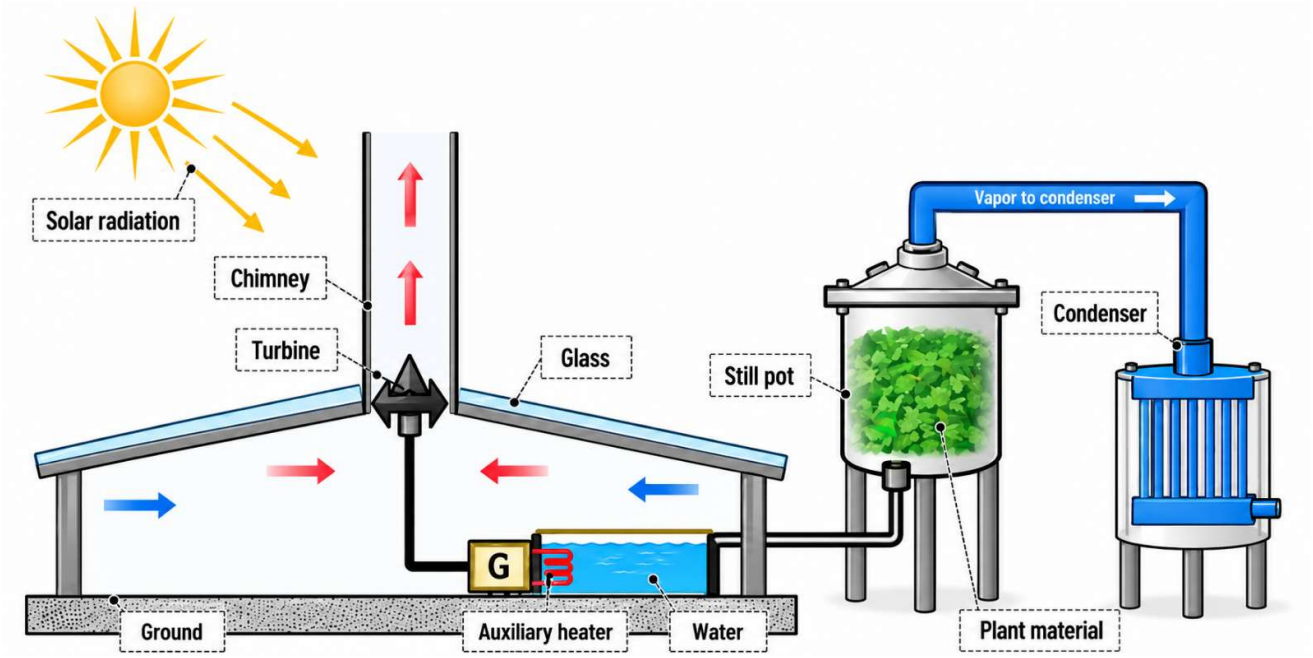


Figure 1: Configuration of the solar chimney still incorporating a partial storage system with auxiliary electrical heating

The operating principle is based on the complementary nature of the two zones. Under solar radiation, the water in the basin gradually heats to its saturation temperature. When solar input becomes insufficient, especially in January, the electric heating element supplements the heat supply. It is powered by the electricity generated in zone B, within the limit of the net power available. Once saturation is reached, additional thermal energy is used to vaporize water. The resulting steam is then directed to the still for essential oil extraction by steam distillation.

The separation of the zones is intended to limit thermofluid interactions between the basin and the main airflow while maintaining energy coupling through auxiliary electrical heating. The objective is to reach saturation during unfavorable periods and maintain steam production for a target extraction duration of four hours. The feasibility of this operation will be evaluated using transient thermal and electrical balances.

The basin is positioned at the collector periphery to reduce interactions with the main airflow and preserve its solar **exposure.** Indeed, in a convergent radial flow, the reduction in flow cross-section toward the chimney tends to increase air velocity near the center. Peripheral positioning thus limits convective exchanges imposed on the basin and possible airflow disturbances. It also aims to reduce shading by the chimney–turbine structure, which could decrease the solar radiation received by the water. Finally, this arrangement leaves the central region available for airflow toward the chimney. These geometric and thermal advantages are examined in the system performance analysis.

2.2. Modeling of the thermoelectric performance of the solar chimney power plant

2.2.1. Modeling assumptions [5], [9], [10], [8], [7]:

To simplify the analysis of thermoelectric performance, the following assumptions are made.

Zone A: Thermal production and vaporization

- The six thermal nodes other than water are treated in a quasi-steady state at each time step. Water is modeled under transient conditions to account for its thermal inertia.
- The immersed electrical heating element provides controlled supplementary heat. Its power is limited by heating demand and the electricity available from zone B.
- The basin retains the characteristics of the previous study: 6 m diameter, 1 cm water depth and Glass–Low-E glazing.
- The steam produced is discharged toward the still. The mass balance accounts for this discharge, with no water replenishment during the reference simulation.

Zone B: Electricity production

- Airflow is assumed to be radial, converging toward the chimney, and described by a one-dimensional aerodynamic model.
- Thermal draft in the chimney drives airflow and provides mechanical power recoverable by the turbine.
- Electrical power is determined from the turbine's mechanical power and conversion efficiencies.

Assumptions for coupling between zones

- The two zones experience the same weather conditions, but their thermal balances are solved separately.
- Decoupling is treated as a modeling assumption, not as perfect physical independence.
- Energy coupling is provided by the electricity produced in zone B and consumed by the heating element in zone A.
- Without a battery or external power supply, auxiliary heating power cannot exceed the net electrical power available at any instant.
- Simulations use a common time step to represent the evolution of temperatures, electricity generation and vaporization simultaneously.

2.2.2. Modeling of heat exchanges and temperatures in the solar chimney

The heat transfer phenomena and the equivalent electrical circuit for heat transfer in the zone A collector are as follows [4], [11], [12]:

International Journal of Progressive Sciences and Technologies (IJPSAT)
ISSN: 2509-0119.
© 2026 Scholar AI LLC.
https://ijpsat.org/
Vol. 60 No. 1 November 2026, pp. 605-625

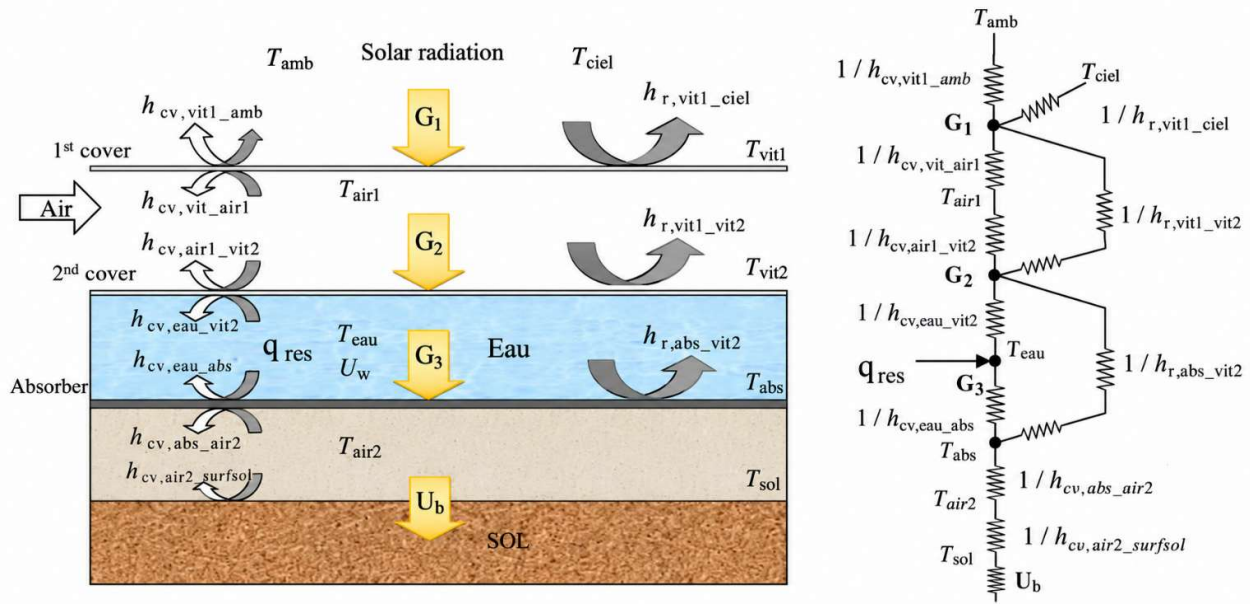


Figure 2: Heat exchange and equivalent electrical circuit for heat transfer in each part of the zone A collector

System of equations with 7 unknowns – zone A:

$$\begin{cases} G_1 + h_{r,vit2_vit1}\left(T_{vit2} - T_{vit1}\right) + h_{cv,vit1_air1}\left(T_{air1} - T_{vit1}\right) = h_{cv,vit1_amb}\left(T_{vit1} - T_{amb}\right) + h_{r,vit1_ciel}\left(T_{vit1} - T_{ciel}\right) \\ h_{cv,vit_air1}\left(T_{vit1} - T_{air1}\right) = h_{cv,vit2_air1}\left(T_{air1} - T_{vit2}\right) \\ G_2 = h_{cv,eau_vit2}\left(T_{eau} - T_{vit2}\right) + h_{cv,air1_vit2}\left(T_{air1} - T_{vit2}\right) + h_{r,vit1_vit2}\left(T_{vit1} - T_{vit2}\right) + h_{r,vit2_abs}\left(T_{vit2} - T_{abs}\right) \\ h_{cv,vit2_eau}\left(T_{vit2}^{k+1} - T_{eau}^{k+1}\right) + h_{cv,eau_abs}\left(T_{abs}^{k+1} - T_{eau}^{k+1}\right) = \rho_e e_e c_{p,e}\dfrac{T_{eau}^{k+1} - T_{eau}^{k}}{\Delta t} + q_{res} \\ G_3 = h_{cv,abs_eau}\left(T_{abs} - T_{eau}\right) + h_{cv,abs_air2}\left(T_{abs} - T_{air2}\right) + h_{r,abs_vit2}\left(T_{abs} - T_{vit2}\right) + U_w\left(T_{abs} - T_{amb}\right) \\ h_{cv,abs_air2}\left(T_{abs} - T_{air2}\right) = h_{cv,air2_surfsol}\left(T_{air2} - T_{surf_sol}\right) \\ h_{r,air_surfsol}\left(T_{air2} - T_{surf_sol}\right) = U_{sol}\left(T_{surf_sol} - T_{sol}\right) \end{cases} \quad (1)$$

Since the basin is sealed, with neither air inlet nor outlet, no air mass flows through it: the air trapped between the glazing and cover remains constant throughout the day. It continues to exchange heat by natural convection with the two adjacent surfaces, but no net flow crosses the node. Consequently, the advective term $\Gamma(T_{air1} - T_{air1,i})$ disappears from equation 2 [13].

Since the basin acts as its own boiler (no water replenishment toward an external system), the auxiliary heater is modeled as a fixed power activated by a threshold (the actual on–off behavior of an immersion heater) [14]:

$$q_{res}(t) = \begin{cases} \dfrac{P_{résistance}}{S_A} \text{ si } T_{eau}(t) \prec T_{consigne} \\ 0 \text{ sinon} \end{cases} \quad (2)$$

International Journal of Progressive Sciences and Technologies (IJPSAT)
ISSN: 2509-0119.
© 2026 Scholar AI LLC.
https://ijpsat.org/
Vol. 60 No. 1 November 2026, pp. 605-625

Heat exchanges within the water layer are estimated using a natural convection correlation based on the Rayleigh and Nusselt numbers. The formulation adopted corresponds to the horizontal form of the correlation proposed by Hollands et al. [15]:

The Rayleigh number is $Ra_e = \frac{g\beta_e \Delta T_e e_e^3}{\nu_e \alpha_e}$ où $\Delta T_e = \max(T_{abs} - T_{pf,0})$ (10)

The Nusselt number used $Nu_e = 1 + 1,44\left(1 - \frac{1708}{Ra_e}\right) + \left[\left(\frac{Ra_e}{5830}\right)^{1/3} - 1\right]_+$ (11) is:

The instantaneous thermal power stored in the basin (dynamic regime), obtained directly from the energy balance for a lumped thermal capacity system, can be expressed as [16]:

$$\dot{Q}_{th,eau}(t) = m_{eau,bac}.c_{p,eau}.\frac{dT_{eau}}{dt} \quad (12)$$

The heat transfer phenomena and the equivalent electrical circuit for heat transfer in the zone B collector are as follows [4]:

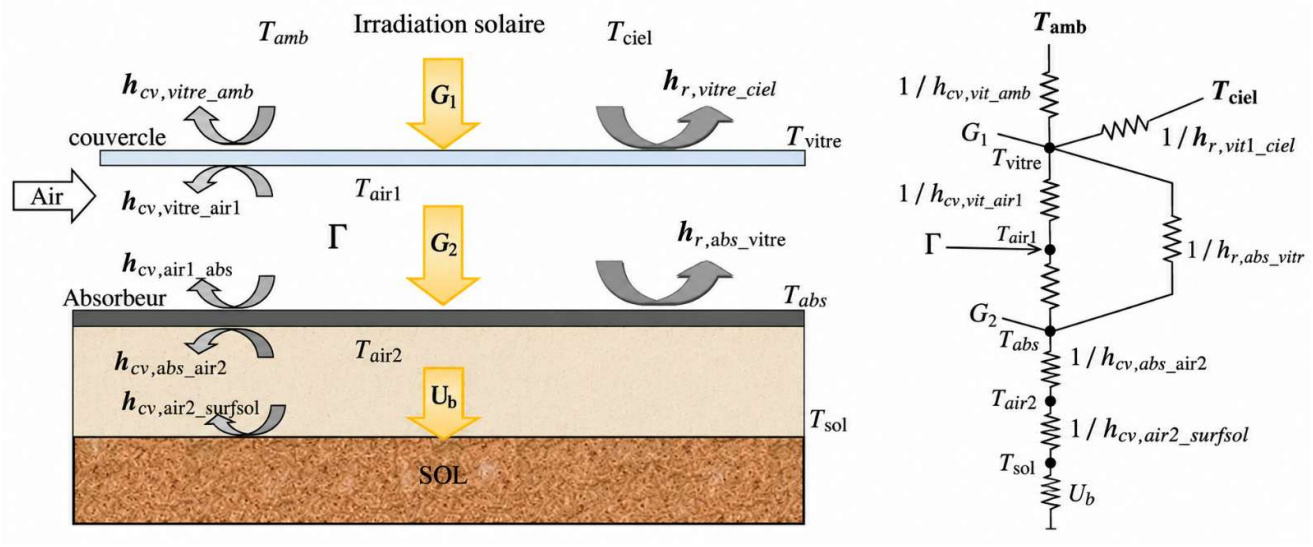


Figure 3: Heat exchange and equivalent electrical circuit for heat transfer in each part of the zone B collector

The system of equations for the temperature distribution in zone B of the collector (system with 5 unknowns) can be written as follows:

$$\begin{cases} G_1 + h_{r,vitre_abs}(T_{abs} - T_{vitre}) + h_{cv,vitre_air1}(T_{air1} - T_{vitre}) = h_{cv,vitre_amb}(T_{vitre} - T_{amb}) + h_{r,vitre_ciel}(T_{vitre} - T_{ciel}) \\ h_{cv,vit_air1}(T_{vitre} - T_{air1}) = h_{cv,abs_air1}(T_{air1} - T_{abs}) + q''_{air} \\ G_3 = h_{cv,abs_air1}(T_{abs} - T_{air1}) + h_{cv,abs_air2}(T_{abs} - T_{air2}) + h_{r,abs_vitre}(T_{abs} - T_{vitre}) \\ h_{cv,abs_air2}(T_{abs} - T_{air2}) = h_{cv,air2_surfsol}(T_{air2} - T_{sol}) \\ h_{r,air_surfsol}(T_{air2} - T_{sol}) = U_{sol}(T_{sol} - T_{sol,0}) \end{cases} \quad (5)$$

International Journal of Progressive Sciences and Technologies (IJPSAT)
ISSN: 2509-0119.
© 2026 Scholar AI LLC.
https://ijpsat.org/
Vol. 60 No. 1 November 2026, pp. 605-625

The net heat flux transferred to the flowing air can be defined in terms of the mean fluid temperature and inlet temperature as follows [4]:

$$q''_{air} = \frac{\dot{m}_{air} C_{p,air}}{\pi r L}(T_{air} - T_{air,ent}); T_{air} = \frac{T_{air,ent} - T_{air,sort}}{2} \quad (6)$$

The heat transfer coefficient in the ground is given by the following relationship [4]:

$$U_{sol} = 2\sqrt{\frac{k_{sol}\rho_{sol}C_{p,sol}}{\pi t}} \quad (7)$$

2.2.3. Energy performance of the solar chimney power plant (zone B)

❖ **Collector thermal efficiency:**

The collector thermal efficiency can be expressed as the ratio of the increase in air thermal power to the solar energy supplied to the collector [17]:

$$\eta_{coll} = \frac{Q_{coll}}{G_{coll}}, \quad \eta_{coll} = \alpha - \frac{\beta}{G_H}\Delta T_{coll} \quad (8)$$

$$\text{Where } Q_{coll} = \dot{m} C_p \Delta T_{coll} = \alpha A_{coll} G_H - \beta A_{coll} \Delta T_{coll} \quad (9)$$

The air mass flow rate at the chimney inlet can be calculated as follows:

$$\dot{m} = \rho_{coll} \times A_{chem} \times V_{air,chem} \quad (10)$$

❖ **Chimney thermal efficiency**

According to Jörg Schlaich, chimney efficiency is expressed as follows [13]:

$$\eta_{chem} = \frac{P_{tot}}{Q_{coll}} = \frac{g \times H_{chem}}{Cp \times T_{amb}} \quad (11)$$

Using the Boussinesq approximation for an ideal gas, the air velocity at the chimney inlet is [18]:

$$V_{ch} = \sqrt{2gH_{chem}\frac{\Delta T}{T_{amb}}}, \quad \Delta T = T_{air1} - T_{amb} \quad (12)$$

The total power of the airflow can be expressed as follows:

$$P_{tot} = \rho_{air} g H_{chem} \frac{\Delta T}{T_{amb}} V_{ch} S_{chem} \quad (13)$$

❖ **Electrical power produced by the** SCPP

According to Schlaich in 1995 [19], this is the net power delivered. It can be expressed as the maximum mechanical power recovered at the turbine shaft multiplied by the turbine efficiency.

International Journal of Progressive Sciences and Technologies (IJPSAT)
ISSN: 2509-0119.
© 2026 Scholar AI LLC.
https://ijpsat.org/
Vol. 60 No. 1 November 2026, pp. 605-625

$$P_{CCS,elec} = \eta_{turb} \times P_{tur,max} \quad (14)$$

The maximum mechanical power extracted by the turbine is obtained when the pressure drop across the turbine equals two-thirds of the total available pressure difference:

$$P_{tur,max} = \frac{2}{3}\eta_{coll}\eta_{chem}G_H A_{coll} \quad (15)$$

Thus, the power generated by the solar chimney is proportional to the collector area and chimney height, and therefore to the volume of a cylinder whose base equals the collector area and whose height equals the chimney height:

$$P_{CCS,elec_max} = \frac{2}{3}\eta_{Turb}\,\eta_{coll}\frac{gH_{chem}}{C_{p,air}T_{amb}}G_H A_{coll} \quad (16)$$

❖ **Overall system efficiency:**

$$\eta_{global} = \frac{P_{elec}}{G.S_{coll}} \quad (17)$$

2.2.4. Simulation parameters

Simulations are carried out for the Mahajanga site using meteorological data covering 2010–2024. January and October are selected as unfavorable and favorable sunshine conditions, respectively. Hourly solar radiation and ambient temperature profiles are used to evaluate the performance of both zones.

Table 1: Geometric parameters of the proposed solar chimney power plant

Parameter	Symbol	Value
Collector diameter	D_{col}	80 m
Basin diameter (Zone A)	D_{bac}	6 m
Collector air-gap height	H_{col}	1,5 m
Chimney height	H_{chem}	100 m
Chimney diameter	D_{chem}	4 m
Water layer thickness	e	0,01 m
Operating pressure	Pb	1 bar absolute
Saturation temperature	Psat	99,61°C
Glazing configuration	--	Glass–Low-E

Auxiliary electrical heating is sized according to the thermal demand of zone A and the net power generated by zone B. Unlike the initial configuration, the rated power of the heating element is not imposed. It is determined from the energy shortfall to reach saturation and maintain a target steam flow rate.

Calculations are performed under transient conditions for water, while the other thermal nodes are solved in quasi-steady state at each time step. Performance is evaluated in terms of time to saturation, steam production, electricity consumption and

International Journal of Progressive Sciences and Technologies (IJPSAT)
ISSN: 2509-0119.
© 2026 Scholar AI LLC.
https://ijpsat.org/
Vol. 60 No. 1 November 2026, pp. 605-625

solar contribution. The main objective is to assess whether steam can be produced for four consecutive hours in January using electricity generated by zone B.

3. RESULTS AND DISCUSSION

3.1. **Meteorological conditions at the Mahajanga site**

Figure 4 shows the evolution of solar radiation and ambient and sky temperatures in Mahajanga in January and October. The data cover 2010–2024.

Solar radiation increases progressively in the morning, peaks around solar noon and then decreases in the afternoon. Maximum values reach 655,57 W·m⁻² in January and 949,57 W·m⁻² in October. This difference reflects more favorable sunshine conditions in October. Ambient and sky temperatures also vary throughout the day, influencing heat exchanges with the surroundings. These meteorological conditions therefore determine solar input and heat losses from the system. January is selected as the unfavorable month for sizing auxiliary electrical heating, while October is the favorable reference month.

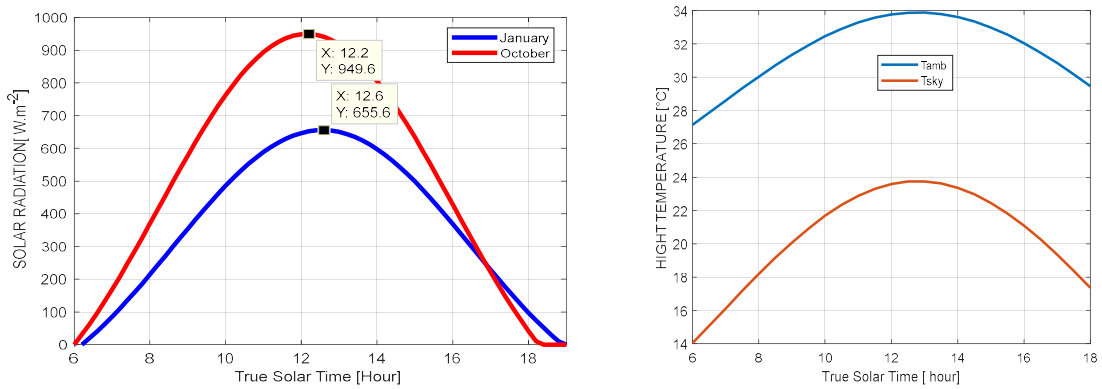


Figure 4: Time evolution of solar radiation and ambient and sky temperatures in January and October

3.2. Influence of basin position on thermal performance

Figure 5 below shows the effect of the basin position under the collector on water temperature and water thermal power. Basin location was evaluated through simulation using the zone A thermal model. To represent a central position, shading by the chimney–turbine structure was considered at three levels, reducing the direct solar radiation received by the basin (50, 80 and 100% shading). Water temperature, initially 100,6 °C in the peripheral position, decreases to 70,9 °C, 45,4 °C and 28,2 °C as shading increases.

The available thermal power follows the same trend, falling from 2,30 kW at the periphery to 1,39 kW, 0,62 kW and 0,10 kW at the different shading levels. These results show that peripheral positioning is not an arbitrary choice but a necessary condition for maintaining direct solar input to the basin. Improved convective exchange due to higher air velocity at the center cannot compensate for the loss of solar radiation when the basin is shaded by the chimney.

International Journal of Progressive Sciences and Technologies (IJPSAT)
ISSN: 2509-0119.
© 2026 Scholar AI LLC.
https://ijpsat.org/
Vol. 60 No. 1 November 2026, pp. 605-625

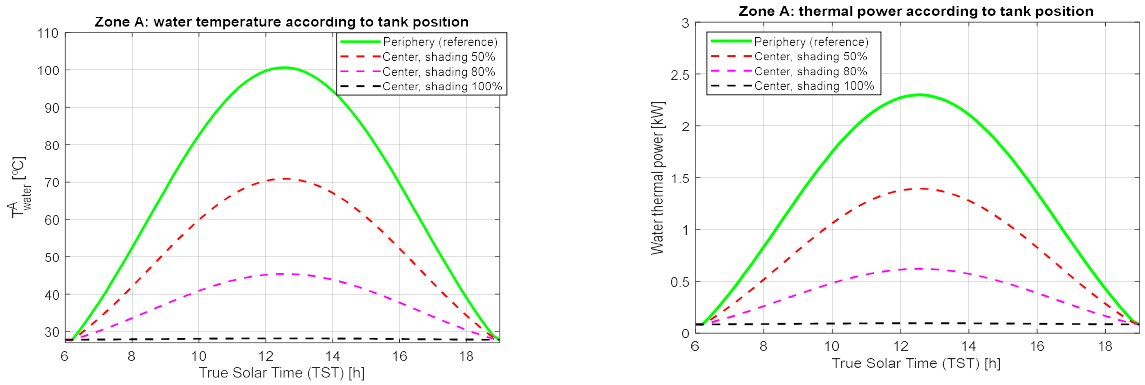


Figure 5: Effect of the water basin position beneath the collector on water temperature and water thermal power

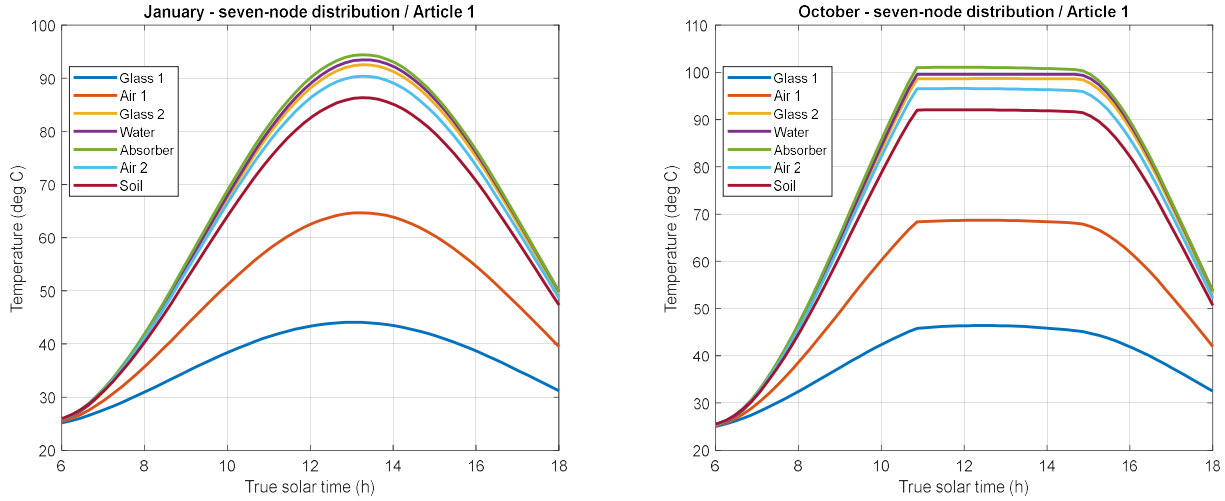
3.3. Energy performance of the solar chimney power plant

3.3.1. Transient thermal performance of zone A

Figure 6 shows the evolution of the seven temperatures in zone A in January and October. Temperatures increase progressively under solar radiation and then decrease in the afternoon. The absorber has the highest temperatures, reaching 94,44 °C in January and 101,07 °C in October. The outer glazing remains the coolest, with respective maxima of 44,09 °C and 46,40 °C, because of heat exchanges with the environment.

Water responds more slowly owing to its thermal inertia. Its maximum temperature reaches 93,48 °C in January without reaching saturation. In October, it reaches 99,61 °C and allows vaporization.

These results highlight the influence of sunlight and thermal inertia on basin behavior. They confirm that without



auxiliary electrical heating, zone A cannot produce boiling steam in January.

Figure 6: Time distribution of the seven temperatures in zone A in January (left) and October (right)

Figure 7 illustrates the evolution of water thermal power in the two months studied. This power depends on heat exchanges between the water and the other collector components. It reaches a maximum of 4,51 kW in January and 6,96 kW in October, at approximately 9 h 27 and 12 h 04 true solar time (TSV), respectively.

International Journal of Progressive Sciences and Technologies (IJPSAT)
ISSN: 2509-0119.
© 2026 Scholar AI LLC.
https://ijpsat.org/
Vol. 60 No. 1 November 2026, pp. 605-625

In January, the heat received gradually warms the water but remains insufficient to reach saturation. The energy accumulated is solely sensible heat, with no steam generated by boiling. In October, greater thermal input allows saturation to be reached. Thereafter, part of the available energy is used for the phase change. Water temperature remains limited to 99,61 °C while vaporization continues. This behavioral difference shows that the thermal power available in January must be supplemented to produce steam for the still.

Figure 8 compares steam production in January and October without auxiliary electrical heating. In January, no boiling steam is produced because water temperature remains below saturation. In October, vaporization begins at 10 h 52 when water reaches 99,61 °C. Cumulative production reaches 31,57 kg, with a maximum mass flow rate of 11,10 $kg.h^{-1}$.

These findings show that zone A can produce steam under favorable conditions but experiences a thermal deficit in January. This limitation justifies investigating supplementary energy input to operate the still during the unfavorable month.

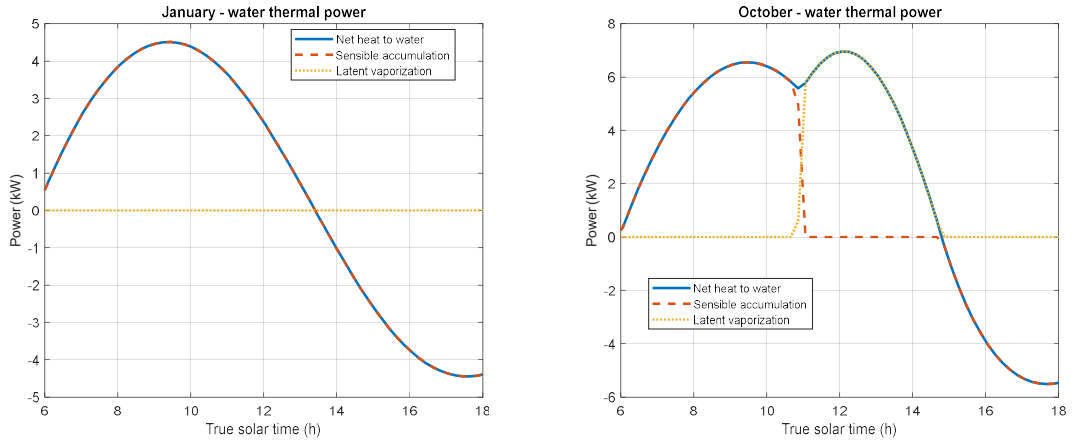


Figure 7: Time evolution of water thermal power in January (left) and October (right).

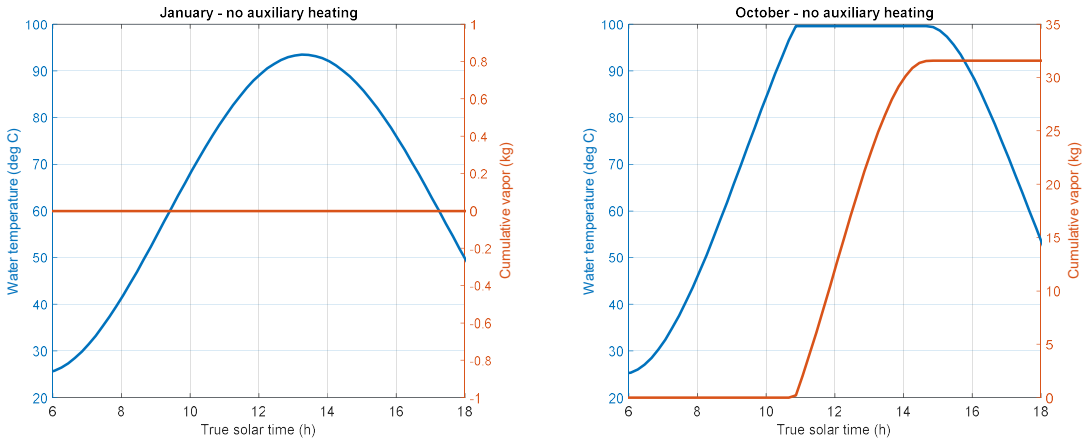


Figure 8: Evolution of water temperature and cumulative steam mass in January (left) and October (right).

International Journal of Progressive Sciences and Technologies (IJPSAT)
ISSN: 2509-0119.
© 2026 Scholar AI LLC.
https://ijpsat.org/
Vol. 60 No. 1 November 2026, pp. 605-625

3.3.2. Energy performance of zone B

❖ **Thermal performance**

Figure 9 shows the evolution of the five temperatures in zone B for January and October. The temperatures increase with solar radiation and reach maxima around solar noon. The absorber has the highest temperatures, 75,18 °C in January and 93,70 °C in October. Flowing air temperature reaches 71,80 °C and 88,94 °C, respectively.

This distribution shows that the absorber transfers part of the heat received to the air circulating under the collector. Air heating promotes thermal draft in the chimney. Higher temperatures in October reflect the effect of sunshine on the thermal performance of zone B.

Figure 10 shows the time evolution of the useful thermal power of air in the collector. It increases in the morning, peaks around solar noon and gradually decreases. Calculated peak powers are 1,96 MW in January and 2,84 MW in October.

In this simulation, the collector thermal efficiency is fixed at 60%. Thermal power therefore varies mainly with incident solar radiation. The increase observed in October results from more favorable sunshine conditions.

This thermal power is the energy resource used to estimate electricity generation by the chimney.

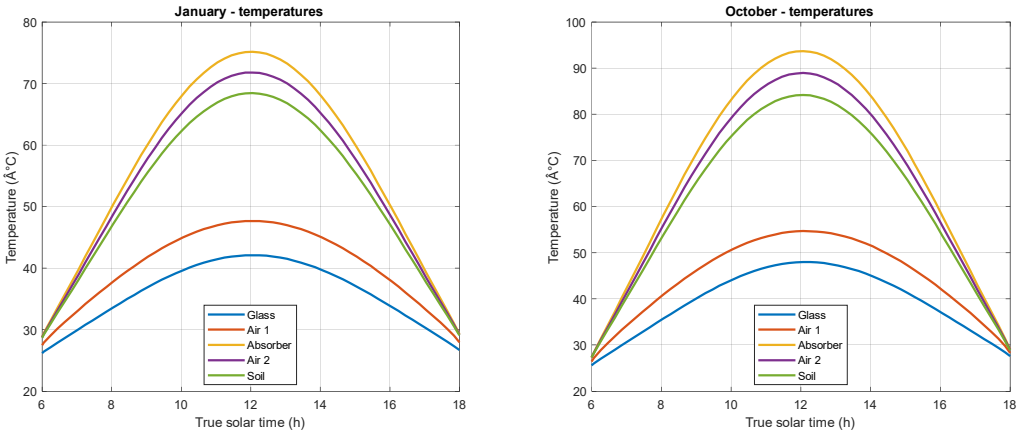


Figure 9: Temperature distribution in collector zone B during the unfavorable and favorable months at our site

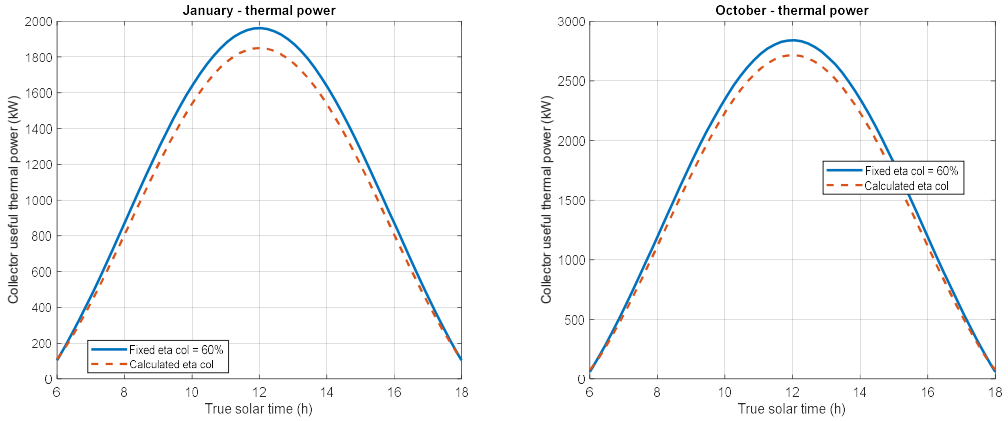


Figure 10: Time evolution of air thermal power in January and October

International Journal of Progressive Sciences and Technologies (IJPSAT)
ISSN: 2509-0119.
© 2026 Scholar AI LLC.
https://ijpsat.org/
Vol. 60 No. 1 November 2026, pp. 605-625

Zone B thus acts as a transfer system: unlike zone A, it does not seek to accumulate energy but instead rapidly conveys it in the form of hot airflow. The two figures complement each other: the temperature distribution highlights the thermal limitation, while air power reflects transfer efficiency.

In summary, zone B operates as a ventilated dry collector, where heat is continuously carried by airflow to the chimney. This dynamic greatly limits temperature rise, unlike zone A, where energy is trapped and stored in the water basin. Comparing the zones thus reveals two complementary thermal approaches: zone A maximizes the accumulation of useful energy, whereas zone B favors its rapid outward transfer.

❖ **Electrical performance:**

Figure 11 illustrates the evolution of generated electrical power and incident solar radiation. Both follow similar time profiles, with maxima near solar noon. In January, maximum electrical power reaches 3,35 kW for irradiance of 655,57 W·m⁻². In October, it reaches 4,81 kW for irradiance of 949,57 W·m⁻². Electrical power therefore increases with the solar energy received.

These results show that electricity generation in zone B is strongly related to solar radiation availability. Its decrease in January constrains the supply of auxiliary electrical heating in zone A.

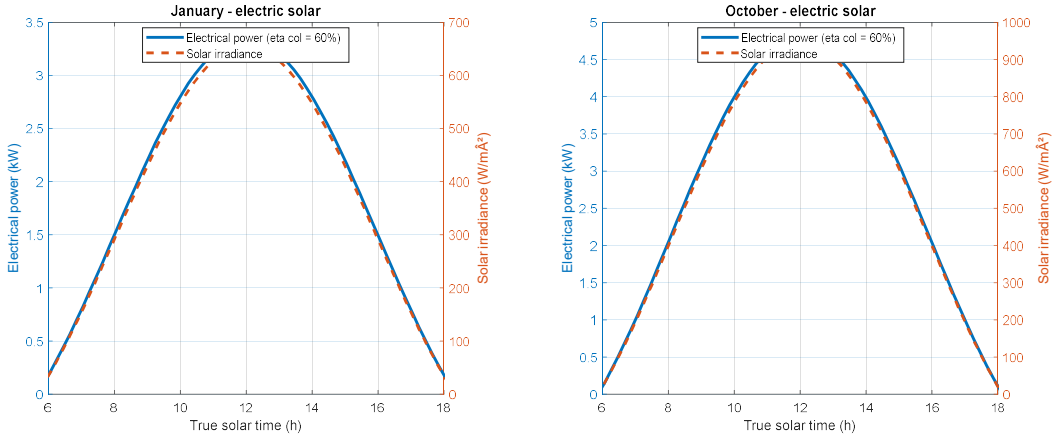


Figure 11: Time evolution of electrical power as a function of solar radiation

This relationship between the two zones explains the significance of decoupling: zone B converts solar radiation directly into electricity (producer), while zone A uses this electricity for thermal extraction through its sealed basin (consumer). Thus, the two zones complement each other not only thermally but also energetically, forming an integrated system in which chimney electricity generation supplies basin consumption. The system then becomes energy-autonomous without requiring an external grid to power auxiliary heating. However, the available electrical power is limited by what zone B can produce and cannot be freely selected.

❖ **Parametric analysis of electrical performance**

Figure 12 shows how geometric and energy parameters influence electrical power production during the unfavorable month in Mahajanga.

- ✓ Influence of chimney height (a): Peak power increases from 2,68 to 4,02 kW when height increases from 80 to 120 m. This increase is explained by improved thermal draft, which increases available mechanical power.
- ✓ Influence of collector diameter (b): As diameter increases from 70 to 100 m, peak power rises from 2,56 to 5,25 kW. This is due to increased collecting area and available solar power.

International Journal of Progressive Sciences and Technologies (IJPSAT)
ISSN: 2509-0119.
© 2026 Scholar AI LLC.
https://ijpsat.org/
Vol. 60 No. 1 November 2026, pp. 605-625

- ✓ Influence of thermal efficiency (c): Increasing the imposed efficiency from 50 to 65% raises peak power from 2,79 to 3,63 kW. This result confirms the effect of useful collector heat on electricity generation.
- ✓ Influence of solar radiation (d): Comparing January, July, October and December profiles gives respective peak powers of 3,35, 3,54, 4,85 and 4,12 kW. October has the highest peak, while January has the lowest production of the four months studied.

Parametric analysis shows that collector diameter and chimney height are two important levers for improving electrical power. These findings guide the sizing of zone B to meet the energy needs of zone A.

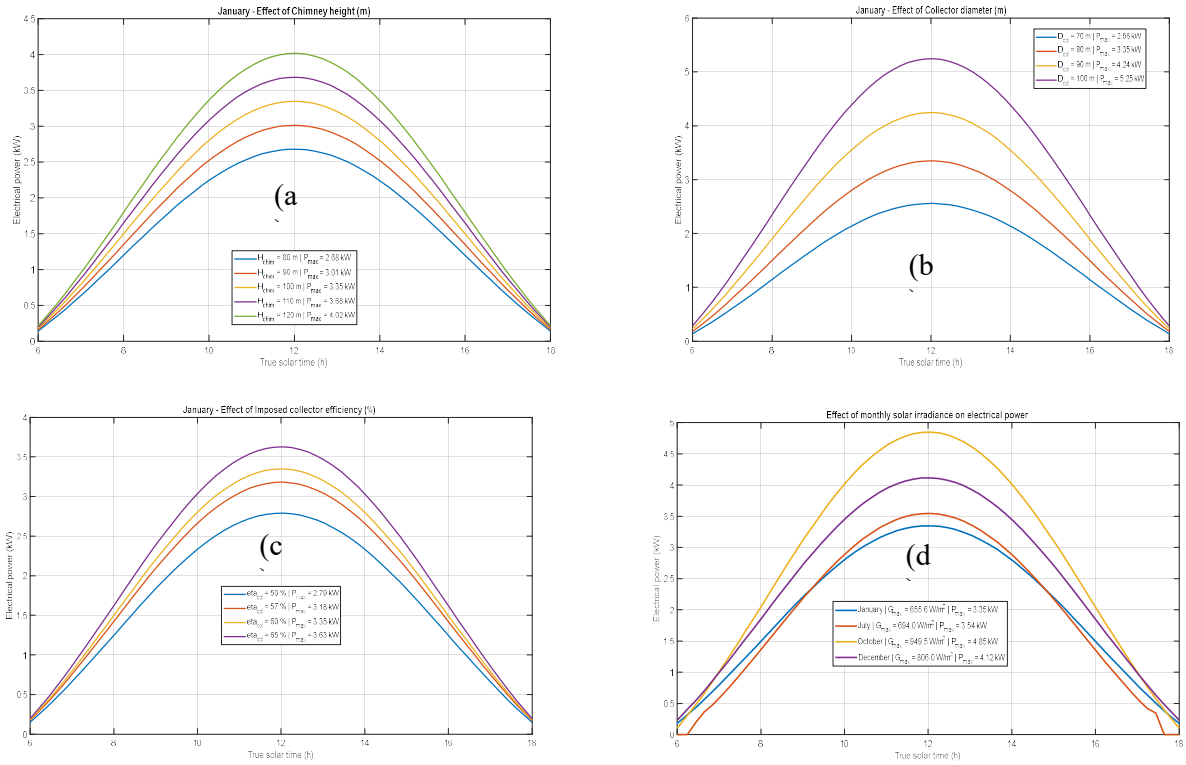


Figure 12: Effects of chimney height (a), collector diameter (b), collector efficiency (c) and the month considered (d) on electrical power as a function of TSV

Figure 13 shows the effects of geometric and climatic parameters on these efficiencies. The results as a whole confirm that warm climates favor collector efficiency (a), but slightly reduce chimney efficiency (b). Moreover, chimney height (90 m to 120 m) appears to be the main lever for improving overall efficiency (c), depending on ambient temperature. Ultimately, the collector is not the limiting factor; the chimney is the structural weakness of the concept, explaining why overall efficiencies of solar chimney power plants remain very low despite effective collectors.

International Journal of Progressive Sciences and Technologies (IJPSAT)
ISSN: 2509-0119.
© 2026 Scholar AI LLC.
https://ijpsat.org/
Vol. 60 No. 1 November 2026, pp. 605-625

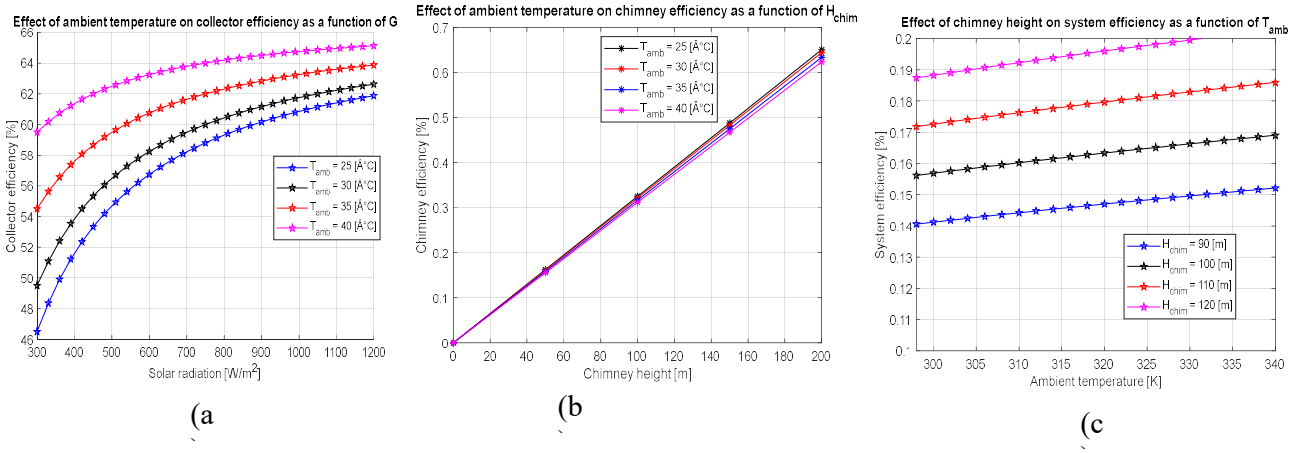


Figure 13: Effect of T_amb on collector efficiency as a function of solar radiation (a), effect of T_amb on chimney efficiency as a function of H_chem (b), and effect of H_chem on system efficiency as a function of T_amb (c).

Analysis of the two zones highlights their complementary functions. Zone A directly converts solar energy into heat and steam, while zone B produces electricity through thermal draft in the chimney.

In January, zone A cannot produce steam without auxiliary electrical heating. Meanwhile, zone B supplies a peak electrical power of 3,35 kW. This production represents a potential resource for compensating for the basin's thermal deficit.

However, electrical power availability varies throughout the day. It must therefore be compared with the actual thermal demand of zone A before sizing the heating element.

3.4. Assessment of the thermal deficit of zone A in January

Transient simulations show that in January, maximum water temperature reaches 93,48 °C at approximately 13 h 15 TSV. It therefore remains below the saturation temperature of 99,61 °C corresponding to 1 bar absolute pressure. The temperature difference is 6,13 °C.

For the 6 m-diameter basin with a 1 cm water layer, the initial mass is 282,74 kg. The sensible energy associated with this difference is estimated at 2,01 kWh.

This value represents the energy needed to raise the water from its natural maximum temperature to saturation at a given instant. It does not account for changes in heat exchanges during supplementary heating.

Sizing the auxiliary heater therefore requires a transient analysis taking into account the desired time to reach saturation and solar power available throughout the day.

Reaching saturation does not guarantee sufficient steam production for extraction. Additional energy is required for phase change and to maintain steam flow for the desired duration.

In October, cumulative natural production reaches 31,57 kg. This value is used as an energy reference to assess system operation in January.

If this quantity is uniformly distributed over four hours, the target average flow rate is 7,89 kg/h. The corresponding latent thermal power is estimated at 4,95 kW.

The results highlight two complementary thermal requirements in January. The first is the sensible energy required to reach saturation. The second is the latent heat needed to maintain steam generation.

The proposed electric heating element has a rated power of 3 kW. It supplements solar input when the latter becomes insufficient.

However, available thermal power varies during the day. Auxiliary heating performance must therefore be evaluated using the basin's instantaneous demand and the electrical power produced by zone B.

3.5. Analysis of the match between thermal demand and electricity generation

Electricity generated by zone B is the energy source for the zone A heating element. In January, electrical power varies throughout the day and peaks at 3,35 kW around solar noon.

The selected heating element has a rated power of 3 kW, lower than the chimney's maximum output. However, available power is lower early and late in the day. Auxiliary operation therefore depends on instantaneous electrical availability.

Energy analysis covers two periods: water preheating from 6 h 00 to 10 h 00 and the target vaporization period from 10 h 00 to 14 h 00.

In January, electrical energy produced by zone B reaches 5,56 kWh between 6 h 00 and 10 h 00 and 12,08 kWh between 10 h 00 and 14 h 00.

To produce a target quantity of 31,57 kg of steam in four hours, the required latent energy is estimated at 19,79 kWh. This is the gross thermal energy needed for vaporization.

Electricity available during the four-hour period remains below this demand. However, solar radiation contributes directly to heating the water. The heating element therefore only needs to provide the supplementary energy required to compensate for the thermal deficit.

Verification of operation thus requires simultaneous consideration of solar input in zone A, available electricity from zone B and system heat losses.

The results show that zones A and B have complementary energy functions. Zone A uses solar radiation directly to heat water, whereas zone B generates the electricity used to supplement this thermal input.

In January, natural solar production is insufficient to reach saturation. However, electrical power supplied by the chimney is a supplementary resource that could improve basin performance.

This analysis justifies including auxiliary heating in the transient model to verify its effects on water temperature, steam production and operating duration.

3.6. Influence of auxiliary electrical heating on zone A performance

3.6.1. Influence of auxiliary electrical heating on water temperature

Figure 14 compares water temperature and cumulative steam mass in January, without and with auxiliary electrical heating. In both configurations, temperature increases progressively in the morning under solar radiation. However, the heating element accelerates water heating and enables saturation at 99,61 °C to be reached around 11 h 51 TSV, whereas the maximum remains limited to 93,48 °C without auxiliary heating.

After saturation is reached, water temperature temporarily stabilizes at 99,61 °C. The available thermal energy then contributes to vaporization rather than to further temperature rise. This evolution is accompanied by a progressive increase in cumulative steam mass, which reaches 6,51 kg around 14 h 03 TSV. Without auxiliary heating, no steam is produced during the day.

From early afternoon onward, decreasing energy input progressively reduces vaporization. When the thermal balance becomes insufficient, the water leaves the saturation plateau and starts cooling.

International Journal of Progressive Sciences and Technologies (IJPSAT)
ISSN: 2509-0119.
© 2026 Scholar AI LLC.
https://ijpsat.org/
Vol. 60 No. 1 November 2026, pp. 605-625

These results confirm that auxiliary electrical heating improves water heating and initiates vaporization during the unfavorable month. However, production remains limited in time and does not yet cover the four hours sought.

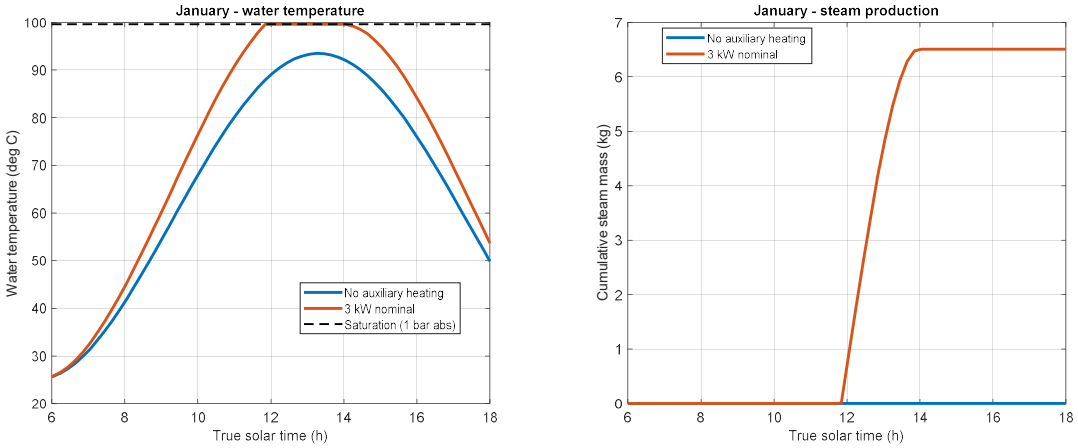


Figure 14: Comparison of the time evolution of water temperature without and with auxiliary electrical heating

3.6.2. Evolution of electrical powers

Figure 15 presents the evolution of electrical power generated by zone B and the power used by the zone A heating element. Both increase progressively in the morning with solar radiation. Electrical generation reaches a maximum of 3,35 kW at approximately 12 h 03 TSV.

When generated power is below 3 kW, the heating element uses the available power. It then reaches its rated value of 3 kW around 10 h 39 TSV and maintains this level until approximately 13 h 27 TSV. During this period, electricity generation in zone B is sufficient to fully supply the element.

After the peak, generated electrical power gradually declines. The heating element can no longer maintain its rated power and follows the reduction in generation. Around 14 h 03 TSV, its effective power falls to 2,82 kW, while vaporization becomes almost zero.

This evolution highlights the dependence of auxiliary electrical heating on instantaneous electricity production from the solar chimney. The rated power of 3 kW is achieved during strong sunshine but cannot be maintained throughout the day.

International Journal of Progressive Sciences and Technologies (IJPSAT)
ISSN: 2509-0119.
© 2026 Scholar AI LLC.
https://ijpsat.org/
Vol. 60 No. 1 November 2026, pp. 605-625

This limitation contributes to the decrease in afternoon steam **production.**

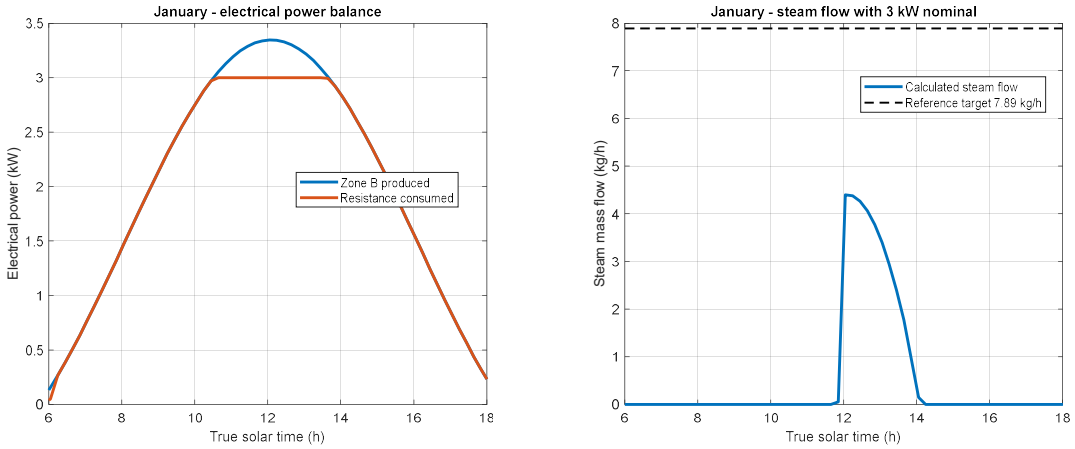


Figure 15: Evolution of electrical power produced by zone B and that supplied by the electric heating element

3.6.3. Distribution of zone A temperatures with auxiliary electrical heating

Figure 16 shows the evolution of the temperatures of the seven thermal nodes in zone A in January with a 3 kW rated electric heating element. Temperatures increase progressively during the morning under the combined effects of solar radiation and electrical heating. The absorber reaches a maximum temperature of 100,62 °C, followed by the inner glazing at 98,58 °C and adjacent air at 96,16 °C. The outer glazing shows the lowest maximum temperature, 45,45 °C, because of heat exchanges with the environment.

Water reaches saturation at 99,61 °C at approximately 11 h 51 TSV, compared with a maximum of 93,48 °C without auxiliary heating. Its temperature then remains constant during vaporization, with available thermal energy mainly used for phase change. This behavior reflects the effect of latent heat, which limits temperature rise despite continued heating.

From the beginning of the afternoon, temperatures of the various components gradually decrease. This is accompanied by a reduction in net thermal power available to the water, which becomes increasingly negative. The electrical contribution can no longer maintain vaporization, resulting in lower steam flow and subsequent cooling of the water.

These results highlight the role of auxiliary electrical heating in reaching saturation and the influence of heat exchanges among components on vaporization duration. They also show that maintaining saturation temperature depends on the balance between energy input and system heat losses.

International Journal of Progressive Sciences and Technologies (IJPSAT)
ISSN: 2509-0119.
© 2026 Scholar AI LLC.
https://ijpsat.org/
Vol. 60 No. 1 November 2026, pp. 605-625

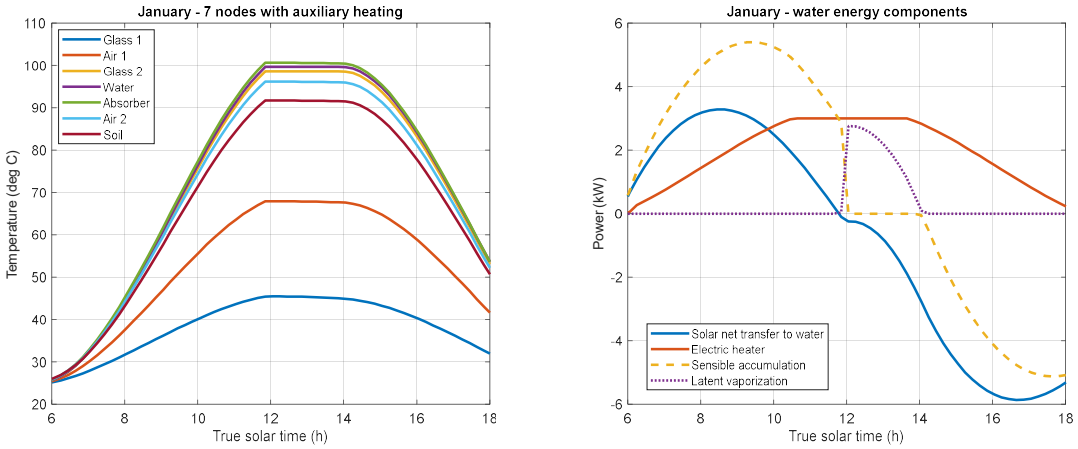


Figure 16: Evolution of the temperatures of the seven thermal nodes in zone A in January, with an electric heating element

Thus, integrating a 3 kW electric heating element substantially improves the thermal performance of zone A in the least favorable month. In January, it enables the saturation temperature of 99,61 °C to be reached, compared with a maximum of only 93,48 °C without auxiliary heating. Thanks to this supplementary input, the system produces 6,51 kg of steam over approximately 2 h 12 min, with a maximum flow rate of 4,40 kg·h⁻¹. However, the gradual decline in electricity generation from zone B, together with decreasing available thermal input, progressively reduces vaporization capacity. Despite this limitation, the results demonstrate that coupling solar thermal and electrical production is a relevant solution for generating steam during periods of low sunshine.

3.6.4. Comparison with experimental extraction trials

The hybrid system's performance was compared with six experimental trials carried out on Niaouli, Kininina and Ravintsara. The comparison is based on extraction durations and mean flow rates estimated from collected condensate.

In January, the 3 kW auxiliary heating system produces 6,51 kg of steam over approximately 2 h 12 min, with a maximum flow rate of 4,40 kg·h⁻¹ and an average rate of about 2,96 kg·h⁻¹ during that period.

These results suggest possible extraction applications, particularly for plants requiring relatively short durations and low steam quantities.

Table 2: Comparison of simulated performance with the six experimental trials

Plant and load	Estimated flow rate (kg/h)	Extraction duration	Comparison with simulation
Niaouli (68 kg)	7,02	2 h 21 min	Estimated flow rate above the simulated maximum; duration longer by 9 min.
Niaouli (96 kg)	3,30	2 h 20 min	Estimated flow rate below the maximum but above the simulated mean; duration longer by 8 min.
Kininina (156,5 kg)	8,82	2 h 16 min	Estimated flow rate above the simulated maximum; duration longer by 4 min.

Kininina (62 kg)	1,08	3 h 15 min	Low estimated flow rate, but duration longer by 1 h 03 min.
Kininina (80 kg)	8,57	2 h 20 min	Débit estimé supérieur au maximum simulé ; durée supérieure de 8 min.
Ravintsara (16 kg)	3,68	1 h 54 min	Compatible duration; estimated flow rate below the maximum but above the simulated mean.

The 16 kg Ravintsara trial has the shortest experimental duration, 1 h 54 min, with an estimated mean flow rate of 3,68 kg·h⁻¹. The 96 kg Niaouli trial has a flow rate of 3,30 kg·h⁻¹ over 2 h 20 min, slightly longer than the simulated period. The 62 kg Kininina trial requires a lower rate of 1,08 kg·h⁻¹, but its extraction duration reaches 3 h 15 min.

The other trials have higher estimated flow rates, ranging from 7,02 to 8,82 kg·h⁻¹, exceeding the calculated maximum flow rate of the hybrid system.

This comparison shows that Ravintsara is an interesting candidate for an experimental application of the system studied. However, the progressive decline in simulated flow does not yet guarantee full coverage of its needs. These findings highlight both the possibilities and limitations of hybrid operation with a 3 kW heating element.

4. CONCLUSION

This study evaluated the thermoelectric performance of a two-zone solar chimney power plant intended to produce steam for essential oil extraction in Mahajanga. The objective was to examine the contribution of a 3 kW auxiliary heater during the unfavorable month without modifying the initial system configuration.

Simulations show that in October, zone A naturally reaches saturation and produces 31,57 kg of steam. In January, maximum water temperature remains limited to 93,48 °C, preventing vaporization. Meanwhile, zone B supplies a peak electrical power of 3,35 kW in January versus 4,81 kW in October.

The electric heating element enables saturation at 99,61 °C to be reached in January and produces 6,51 kg of steam over approximately 2 h 12 min, with a maximum rate of 4,40 kg·h⁻¹. Auxiliary heating thus improves thermal performance without achieving the four hours of vaporization initially sought.

Comparison with experimental trials shows that Ravintsara, extracted over 1 h 54 min with an estimated mean flow rate of 3,68 kg·h⁻¹, is a potentially interesting application. Nevertheless, the gradual decrease in simulated steam flow does not yet guarantee full coverage of the process requirements.

The results obtained show that combining solar heat and electricity generation is an interesting solution for improving steam availability, even during periods of low sunshine. This complementarity improves process continuity and strengthens overall system performance.

In future work, it would be appropriate to adjust the installation dimensions to the specific requirements of the various plants treated, in order to optimize process energy efficiency and improve profitability.

REFERENCES:

[1] RALEVAMANANA Félix, Evolution des systèmes de distillation traditionnelle d'huile essentielle des feuilles de girofle - contribution à l'étude d'amélioration de foyer d'alambic traditionnel, Mémoire de fin d'études en vue de l'obtention du diplôme de licence en Science et Ingénierie de Matériaux, UNIVERSITE D'ANTANANARIVO, 27 Janvier 2021

[2] Abdelhalim Assassi, Meriem Hafidha Titi, Integration of the Manzanares Solar Chimney Power Plants in Towers: Collector and Building Height Configuration, Engineering, Technology & Applied Science Research Vol. 15, No. 3, 2025, 23002-23007

[3] Marco Aure´lio dos Santos Bernardesa, Xinping Zhoub, On the heat storage in Solar Updraft Tower collectors– Water bags, 27 February 2013

[4]. M. SEMAI Hakim, Recherche d'une configuration optimale d'une centrale solaire à cheminée, 2017.

[1] Duffie, J. A., & Beckman, W. A. (2013). Solar Engineering of Thermal Processes, 4th ed., Wiley

[2] Hollands, K. G. T., Unny, T. E., Raithby, G. D., & Konicek, L. (1976). Free Convective Heat Transfer Across Inclined Air Layers. Journal of Heat Transfer, 98(2), 189–193.

[7] Duffie, J.A., Beckman, W.A. Solar Engineering of Thermal Processes. Wiley-Interscience (éditions successives, 2e éd. 1991).

[8] Ahmadreza Ayoobi and Mahdi Ramezanizadeh, A detailed review investigating the mathematical modeling of solar stills, Frontiers in Energy Research, 25 April 2022

[9] Bernardes, M. A. S., & Zhou, X. (2013). On the heat storage in Solar Updraft Tower collectors – Water bags. Solar Energy, 91, 22–31.

[10] Schlaich, J., Bergermann, R., Schiel, W., & Weinrebe, G. (2005). Design of Commercial Solar Updraft Tower Systems—Utilization of Solar Induced Convective Flows for Power Generation. Journal of Solar Energy Engineering, 127(1), 117–124.

[11] Khalilian, M. (2017). Experimental investigation and theoretical modelling of heat transfer in circular solar ponds by lumped capacitance model. Applied Thermal Engineering, 121, 737–749.

[12] Gortych, M., Lipnicki, Z., Małolepszy, T., & Grabas, P. (2024). Solar Chimney Operation Variant. Energies, 17(19), 5004.

[13] Hollands, K.G.T., Unny, T.E., Raithby, G.D., Konicek, L. (1976). Free convective heat transfer across inclined air layers. *ASME* Journal of Heat Transfer, 98(2), 189-193.

[14] I.ZEGHIB a, A.CHAKER, Simulation of a solar domestic water heating system, Laboratoire Physique Energétique, Université Mentouri Constantine 25000, Algeria, Energy Procedia 6 (2011) 292–301

[15] Hollands, K. G. T., Raithby, G. D., & Konicek, L. (1975). International Journal of Heat and Mass Transfer, 18(7–8), 879–884.

[16] Bergman, T. L., Lavine, A. S., Incropera, F. P., & DeWitt, D. P. Fundamentals of Heat and Mass Transfer.

[17] Dai YJ, Huang HB, Wang NRZ. Case study of solar chimney power plants in North-western regions of China. Renewable Energy 2003 ; 28 : 1295-304.

[18] Soukaina HILALI, Thermal solar energy applications on ecoextraction and drying of orange peels and rosemary leaves, 2020

[19] R. BARISON James, Production d'electricite par une cheminee solaire, Memoire, Université d'Antananarivo, 2012.

[20] ACHOURI El Hadj, Contribution à l'étude expérimentale d'une cheminée solaire en Algérie, these de doctorat, Université Kasdi Merbah Ouargla, 2021